Bull Math Biol (2011) 73: 1529–1558
DOI 10.1007/s11538-010-9578-4

ORIGINAL ARTICLE

How Does Cellular Contact Affect Differentiation Mediated Pattern Formation?

J.M. Bloomfield · K.J. Painter · J.A. Sherratt

Received: 5 January 2010 / Accepted: 3 August 2010 / Published online: 27 August 2010

Abstract In this paper, we present a two-population continuous integro-differential model of cell differentiation, using a non-local term to describe the influence of the local environment on differentiation. We investigate three different versions of the model, with differentiation being cell autonomous, regulated via a community effect, or weakly dependent on the local cellular environment. We consider the spatial patterns that such different modes of differentiation produce, and investigate the formation of both stripes and spots by the model. We show that pattern formation only occurs when differentiation is regulated by a strong community effect. In this case, permanent spatial patterns only occur under a precise relationship between the parameters characterising cell dynamics, although transient patterns can persist for biologically relevant timescales when this condition is relaxed. In all cases, the long-lived patterns consist only of stripes, not spots.

Keywords Community effect · Differentiation · Pattern formation · Mathematical model · Zebrafish · Non-local · Integro-differential equation

1 Introduction

Cellular differentiation describes the development of specialised cells from undeveloped precursor cells. This process occurs in nearly all cells but the mechanisms that

J.M. Bloomfield (✉) · K.J. Painter · J.A. Sherratt
Department of Mathematics and the Maxwell Institute for Mathematical Sciences,
School of Mathematical and Computer Sciences, Heriot Watt University, Edinburgh, EH14 4AS, UK
e-mail: jmb7@hw.ac.uk

K.J. Painter
e-mail: K.J.Painter@ma.hw.ac.uk

J.A. Sherratt
e-mail: J.A.Sherratt@ma.hw.ac.uk

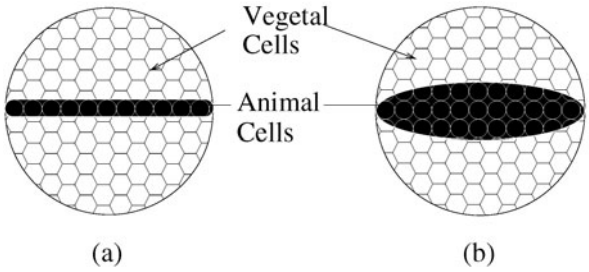

Fig. 1 Schematic of the sandwich experiments originally carried out by Gurdon (1988) to demonstrate the community effect. Part (**a**) shows a monolayer of blastula derived animal cells in a vegetal sandwich, while part (**b**) shows a solid grouping. Gurdon saw differentiation take place only in the latter case. See Gurdon (1988) for more details

drive it are not well understood. Further investigation is necessary to increase our understanding of this fundamental process.

There are many ways that differentiation is induced in cells. For example, it has been widely hypothesised that a cell may sometimes differentiate according to a "community effect". This term was first coined by Gurdon (1988) to explain the phenomenon seen in experiments in which clusters of cells differentiate into a particular tissue type, but individual cells from the same undifferentiated group do not (Gurdon 1988). Gurdon postulated that undifferentiated cells, which receive signals from other undifferentiated cells in the immediate environment, will differentiate together into the same cell type once a threshold level of these signals is reached. This process allows cells in the same spatial area to keep the correct gene expression necessary for the tissue they create. The community effect has since been widely investigated, with many studies expanding on Gurdon's original experiment and explanation. In his original experiments, Gurdon (1988) placed *Xenopus* ectoderm cells in a sandwich of endoderm (see Fig. 1). A monolayer of ectodermal cells did not differentiate into muscle, whereas a solid group of cells did. Gurdon and colleagues went on to explore other similar experiments in *Xenopus*, all with the same results (Kato and Gurdon 1993; Gurdon et al. 1993b). Similar experiments with blastula cells of zebrafish and dorsal ectoderm cells of Drosophila were also carried out (reviewed by Gurdon et al. 1993a). They too showed that groups of cells were needed for the normal differentiation fate of these cells to be achieved.

Weston et al. (1994) explored a different cell group within *Xenopus* to see if cells other than those fated to differentiate into muscle were also driven by the community effect. They studied *Xenopus* notochord, and through sandwich experiments similar to those described above, they concluded that a community effect was also necessary for notochord differentiation. Meanwhile, Cossu et al. (1995) discovered a community effect in mouse myoblast differentiation (Cossu et al. 1995). Work on mice continued, and a community effect was observed at work in the survival of melanoblasts (Aubin-Houzelstein et al. 1998), and even postulated as a possible explanation for the correct migration of Purkinje cells in the cerebellar cortex of mice (Yang et al. 2002), taking the concept of the community effect a long way from its original definition.

Experimental work on a community effect continues, with the latest work looking at cardiomyonocite cells and heartbeat stabilisation (Kaneko et al. 2007; Kojima et al. 2006), but even though a community effect has been explored for over 20 years there

are still some fundamental questions that remain unanswered. One of these is how a community effect is achieved biochemically, and this question has been considered to some extent both experimentally and theoretically. Kim et al. (1999) postulated that neuregulin may act as an induction signal for the community effect in myogenic differentiation in rats, while eFGF protein is suggested as the likely factor in *Xenopus* (Standley et al. 2001). Various other community factors have been suggested for different cells and species (see Buckingham 2003 for a review). Meanwhile in his theoretical paper, Monk (1997) created continuous diffusion-based models to explore mechanisms for the community effect in *Xenopus* myogenesis. The biochemical basis of a community effect remains an important research question, but we do not consider it further in this paper.

Rather, we focus on what the community effect means for the spatial structure of tissues; more concretely, what kind of spatial structure does the community effect permit that other forms of differentiation do not? This question has not previously been explored, with research effort concentrated on the underlying biochemistry. However, it is an important question, as answering it will give insight into the geometries of tissues that the community effect can construct and, conversely, those that it cannot. We begin by briefly considering various forms of differentiation, before moving on to look at the community effect in the context of a specific example.

As mentioned above, cell differentiation is not always regulated by the community effect. For example, "autonomous differentiation" may occur at a certain stage in the cell cycle. In this scenario, the local environment of a cell has no effect on its fate; the cell's progress is intrinsic (Salazar-Ciudad et al. 2003). An example of this is the differentiation of mature somites (Buckingham 2003).

Homoiogenetic induction is another method of inducing differentiation. Here, cells induced to differentiate first self-induce a signal to send to their neighbours, instructing those cells to do the same. In this way, the signal is passed from cell to cell, until such time has lapsed that any undifferentiated cells no longer respond. This process, like the community effect, allows a sharp boundary to be formed between different tissues; for example, it has been suggested as an explanation for the formation of spatial patterns seen in the neural plate of amphibians (Nieuwkoop 1997).

However, as we are interested mainly in a community effect, and the influence it has on the spatial structure of tissue, we focus on that phenomenon here, paying particular attention to the example of a community effect in zebrafish pigmentation. While Gurdon et al. (1993a) provides a very precise definition of the community effect, stating that it is "an interaction among many nearby progenitor cells, as a result of which these cells activate tissue-specific genes and differentiate coordinately as a uniform population", the term has picked up a wider, more general use, as seen in the literature discussed above. In the case of zebrafish pigmentation, the term has been used to describe the preference of pigment cells for their own kind.

The stripes on adult zebrafish form during metamorphosis, which begins at about 14 days post fertilisation (Parichy et al. 2000). The stripes are mainly made up of two cell types, melanophores (black) and xanthophores (yellow), while iridiphores (translucent) are found spread across the body. These pigmented cells, or chromatophores, arise from latent precursors during metamorphosis. These form black and yellow horizontal stripes across the body of the zebrafish, creating two

melanophore stripes by 28 days (Parichy et al. 2000). It has been postulated that the death of melanophores in areas of high xanthophore density is due to a community effect: melanophores require other melanophores nearby in order to survive, and a sole melanophore is not viable (Parichy et al. 2000; Buckingham 2003). This suggests that an undifferentiated precursor will be biased into differentiating into the same type as those differentiated pigment cells surrounding it, as otherwise it will fail to survive.

It is worth noting that biological experiments such as the sandwich experiments described above (see Fig. 1) are intrinsically disruptive. *In vitro* experiments remove cells from their natural environment, and while the *in vivo* grafting of cells may produce useful results, it also alters the natural cellular environment. This leads to potential discrepancies in the interpretation of experimental results (see Nagai et al. 2005, for a discussion of this in zebrafish blastoderm transplantation). Therefore, in order to further understand and isolate the basic process of cell differentiation, we turn to theoretical models.

We are aware of only one previous theoretical model for the regulation of spatial structure by the community effect, which concerns the zebrafish pigmentation example. Moreira and Deutsch (2005) created a cellular automata model which combines ideas about a community effect with those of attraction and repulsion between melanophores and xanthophores. In their model, a cell will differentiate into a melanophore unless there are more xanthophores in the neighbourhood, in which case a xanthophore will arise. The model successfully reproduces the stripe patterns of the zebrafish.

In this paper, we offer an integro-differential equation model to describe cell differentiation. In contrast to Moreira and Deutsch (2005), who assume intercellular adhesion and precursor cell differentiation to be simultaneous drivers for the pattern formation process, we explore what dynamics can be produced through differentiation alone, without considering any adhesive effects. In this way, we are able to explore the extent to which the community effect alone is able to produce the patterns seen in zebrafish patterning.

In Sect. 2, we present the model alongside a comprehensive biological reasoning for its formulation, basing our ideas on the example of zebrafish pigmentation. From this model, we create three variations to explore various differentiation scenarios, looking in particular at a community effect and the strength of the response needed in order to create patterning. In Sect. 3, we go on to consider the stability of the homogeneous steady states of the model, and present various mathematical analyses of them. In Sect. 4, we present the results of numerical simulations, while in Sect. 5 we discuss the outcome of these results. We will show that regulation of differentiation by a strong community effect can generate spatial patterns. The patterns always consist of stripes rather than spots. *De novo* pattern formation only occurs for some initial conditions, showing that regulation of differentiation via a community effect is not a robust pattern formation mechanism. However, it is an effective mechanism for pattern maintenance, provided that the death rates of the two cell populations involved are relatively similar. Note that our model of a community effect assumes that differentiation is only influenced by the local environment and not by any other predisposition toward a particular cell type, so that differentiation rates for this case

are always equal across the two populations. We will show that permanent patterns require equal death rates, but that long-lived transient patterns occur when the death rates of the two cell populations are different but relatively close to one another.

2 Modelling Cellular Differentiation: A Continuous Approach

As mentioned in Sect. 1, cell differentiation is a complex process. We build our model by considering the biological data available. In the development of our model, we bear in mind the particular example of zebrafish pigmentation, although the model we produce is general enough to be applied to many other scenarios, some of which are discussed at the end of this paper. We begin by considering a stem cell population that is both constant in space and time, and multi-potent. To explain these two assumptions, we describe the nature of stem cells, and also cite some evidence that a community effect has a role in the final cell fate of precursors produced from multipotent stem cells. Furthermore, we consider available data regarding the specific case of zebrafish.

In epithelia, stem cells lie in the basal layer. Unlike other cells, stem cells do not terminally differentiate, but rather undergo repeated proliferation. After mitosis, in place of one stem cell, there is typically one stem cell and one undifferentiated cell, with the latter differentiating and joining the general cell population. Stem cells have in some cases been shown to be multi-potent, i.e. the precursor cell that a stem cell produces can have a variety of different fates. These precursors may be multipotent themselves, and, in the peripheral nervous system for example, they are seen to display fate restrictions due to a community effect (Paratore et al. 2002; see also Galli et al. (2000) for further discussions of multi-potency in stem cells and precursor cells, and of the role of a community effect in affecting cell fates in neural stem cells). Note that in the case of zebrafish, it is not known whether the precursors of chromatophores are stem cells or not, although there has been some recent evidence to suggest that they are (Hultman and Johnson 2010). Whether the precursors are multi-potent or not is also unknown, despite speculation on this point (Parichy 2007).

In the creation of a general model then, we first begin with separate stem and precursor cell populations. We assume that we have a stem cell population that remains at a constant level due to self-renewal. We further assume that it produces precursor cells at a constant rate, and that each time a precursor cell differentiates, a stem cell produces a new precursor. In this way, a constant supply of precursor cells is achieved, leading to the population of precursor cells having a constant density p, say, independent of both space and time. Note that we assume that the precursor cells are evenly distributed across the body. In the zebrafish example, although the spatial distribution of precursors across the fish body has not yet been elucidated, in the fin they have been shown to be evenly distributed (Rawls and Johnson 2000), and so we believe this to be a reasonable assumption.

We now look in detail at our terminally differentiated cells: we assume there to be two populations, similar to the melanophores and xanthophores found in zebrafish. We call these two differentiated cell populations $a(x,t)$ and $b(x,t)$, with

$$\frac{\partial a}{\partial t} = k_1 f_1\big(a(p), b(p)\big) - \tilde{\alpha}_1 a(p), \qquad \frac{\partial b}{\partial t} = k_2 f_2\big(a(p), b(p)\big) - \tilde{\alpha}_2 b(p). \quad (1)$$

Note that the coefficients in the two linear death terms generally differ since the cell populations A and B are different. Both a and b depend on p, which determines the rate at which precursor cells differentiate into A or B cells. But from the above discussion, we have that the rate of differentiation of precursor cells is constant, and thus

$$k_1 f_1\big(a(p), b(p)\big) + k_2 f_2\big(a(p), b(p)\big) = \tilde{\alpha}_0 p, \quad \text{say, a constant.} \tag{2}$$

We now investigate further the differentiation functions f_1 and f_2 of our model. As discussed in Sect. 1, the type of cell that the precursor cell differentiates into may depend very much on the differentiated cells in the local environment, or on a cell's predisposition toward a particular cell type. We will explore three options: autonomous cell differentiation, differentiation according to a community effect, and a third option, in which the response to the ratio of existing differentiated cell types in the local environment is strictly linear.

Bearing the above three scenarios in mind, we propose three different forms for the f_1 and f_2 functions, all satisfying (2). Since in each case we wish both cell lines A and B to be produced by the same mode of differentiation, we assume that $f_1(a, b) = f_2(b, a)$. We wish to consider the extent to which the surrounding environment affects the differentiation of precursor cells. We assume that only cells of type A and B affect the fate decisions of the precursor cells. To consider this effect, we first construct an integral which calculates the proportion of differentiated A and B cells within a certain radius R. Such a representation of cell environment via an integral term has been used previously in many contexts including cell sorting (Armstrong et al. 2006), development (Sekimura et al. 1999; Armstrong et al. 2009; Green et al. 2010; Bloomfield et al. 2010), chemotaxis (Hillen and Painter 2009) and cancer (Gerisch and Chaplain 2008; Sherratt et al. 2009; Painter et al. 2010). The cell sensing radius R of the integral reflects the capacity of a cell to directly sense its environment via, for example filopodial contact. The amount of contact made is important as it determines the extracellular signals that a cell receives. For example, Numb is a signalling protein that is widely expressed during embryogenesis. Numb is thought to inhibit Notch activity, thereby altering communication between an undifferentiated precursor cell and other cells in its local environment. This changed level of communication then allows the precursor cell to choose a different fate to that of a second precursor cell which may contain a different amount of Numb, and hence experiences a different level of cell-cell communication (Zhong 2008). We use a function $f(I)$, where I is our local environment integral, to vary the contact and communication of precursor cells with differentiated cells.

Our model in one dimension is given by

$$\begin{aligned} \frac{\partial a}{\partial t} &= k_1 f(I_a) - \tilde{\alpha}_1 a, \quad I_a = \frac{1}{\text{area}} \int_{-R}^{R} \frac{a(x+x_0)}{a(x+x_0)+b(x+x_0)}\, dx_0, \\ \frac{\partial b}{\partial t} &= k_2 f(I_b) - \tilde{\alpha}_2 b, \quad I_b = \frac{1}{\text{area}} \int_{-R}^{R} \frac{b(x+x_0)}{a(x+x_0)+b(x+x_0)}\, dx_0. \end{aligned} \tag{3}$$

Note that in this model, the integrals I_a and $I_b \in [0, 1]$ since they consider the proportion of A or B cells in the sensing region of a cell; moreover $I_a + I_b = 1$. The integral is normalised over the area. Typically, this is simply the length $2R$, but near the edge of the spatial domain being considered, we truncate the integral over the portion of area which lies within our domain. Equations (3) can be non-dimensionalised: substituting $t = t^* P/\tilde{\alpha}_0 p$, $a = a^* P$, $b = b^* P$, $\tilde{\alpha}_1 = \alpha_1 \tilde{\alpha}_0 p/P$, $\tilde{\alpha}_2 = \alpha_2 \tilde{\alpha}_0 p/P$, $k_2/k_1 = k^*$, $f(\cdot) = f(\cdot)^* \tilde{\alpha}_0 p/k_1$, where P is the dimensionalised measure of the cell population density, and dropping the $*$'s, gives $\partial a/\partial t = f(I_a) - \alpha_1 a$ and $\partial b/\partial t = k f(I_b) - \alpha_2 b$, with condition (2) becoming

$$f(I_a) + k f(I_b) = 1. \tag{4}$$

The dimensionless parameter k reflects a possible predisposition of precursor cells to differentiate into cells of type A ($k < 1$) or B ($k > 1$); except where specifically stated, we will restrict our attention to the unbiased case $k = 1$.

Note that the integral I is undefined if $a = b = 0$. Since we are modelling the differentiation of precursor cells into A and B cells from an initial precursor cell layer, the case $a = b = 0$ is definitely relevant in applications. A reasonable assumption is that precursor cells would differentiate into cells of type A and B at equal rates in this case. Therefore, we could amend the model to cover the case $a = b = 0$ via a differentiation function that varied between $1/2$ and $f(I_a)$ (for cell type A) as the overall cell density increased. Such an alteration would be a significant complication mathematically, and would be important for the transient behaviour of populations with low initial density. However, it would not affect long term behaviours, and so we restrict our attention to a model of the form (3).

To more fully represent epithelia, which we model as a monolayer, we extend (3) to two dimensions. The complete dimensionless equations are then

$$\begin{aligned}
\frac{\partial a}{\partial t} &= f(I_a) - \alpha_1 a, \\
I_a &= \frac{1}{\text{area}} \int_0^R \int_0^{2\pi} \frac{a(\underline{x} + r\underline{\eta})}{a(\underline{x} + r\underline{\eta}) + b(\underline{x} + r\underline{\eta})} r \, d\theta \, dr \\
\frac{\partial b}{\partial t} &= k f(I_b) - \alpha_2 b, \\
I_b &= \frac{1}{\text{area}} \int_0^R \int_0^{2\pi} \frac{b(\underline{x} + r\underline{\eta})}{a(\underline{x} + r\underline{\eta}) + b(\underline{x} + r\underline{\eta})} r \, d\theta \, dr.
\end{aligned} \tag{5}$$

Here, $a(\underline{x}, t)$ and $b(\underline{x}, t)$ are our populations of cell types A and B, respectively, at two-dimensional position $\underline{x}$ and time t; other cells within I_a and I_b are located relative to $a(\underline{x}, t)$ and $b(\underline{x}, t)$ by reference to both the distance r along the sensing radius R, and the unit vector $\underline{\eta} = (\cos\theta, \sin\theta)$; α_1 and α_2 are our non-dimensional death rates and k is the non-dimensional differentiation rate; and finally the integral is normalised over the area of the integration region, which is πR^2 at points away from the boundaries of the domain, and truncated appropriately at points whose distance from the boundaries is less than R. The function f is different for our three differentiation scenarios, and we discuss its form below.

2.1 The Three Models

2.1.1 Model One: Differentiation is Independent of the Local Environment

First, we consider cell autonomous differentiation. In this scenario, differentiation into A or B cells will simply occur at a constant rate, predetermined by various internal cell factors such as the presence of different gene regulatory proteins, without reference to the local environment. Such a mechanism occurs in mature somites which are differentiating into muscle (see, for example Buckingham 2003). Differentiation into the two cell types is assumed to occur at different rates, so we allow $k \neq 1$ for this model. We put $f(I_a) = f(I_b)$ a constant, which must equal $1/(1+k)$ to satisfy condition (4). Then (5) becomes

$$\frac{da(t)}{dt} = 1/(1+k) - \alpha_1 a(t) \quad \text{and} \quad \frac{db(t)}{dt} = k/(1+k) - \alpha_2 b(t). \tag{6}$$

We call this our *Cell Autonomous Model*.

2.1.2 Models Two and Three: Differentiation is Dependent on the Local Environment

We now turn to modelling a community effect. Unlike in the autonomous case, we fix $k = 1$, as we do not wish precursor cells to have a predisposition to differentiate into one cell type over another, i.e. we wish differentiation to be only affected by the local environment. The mathematical formulation of f requires only that (i) f is monotonically increasing, so that a larger proportion of cell type A, say, in the sensing region makes it more likely that a precursor cell will differentiate into A; and (ii) $f(I_a) = 1 - f(I_b)$, with $f(1/2) = 1/2$, to avoid any bias between the two cell types. Condition (4) is then immediately satisfied.

To model a strong community effect, we are interested in an f which, although continuous, is close to a step function. We choose f as described in Fig. 2(a). This represents the idea that an undifferentiated precursor cell is strongly biased toward differentiating into the same type as those in the majority around it, as occurs in the community effect described in Sect. 1. We call this version of the model the *Community Model*, and it is given by

$$\frac{\partial a}{\partial t} = f(I_a) - \alpha_1 a \quad \text{and} \quad \frac{\partial b}{\partial t} = f(I_b) - \alpha_2 b, \tag{7}$$

with I_a, I_b and all other details as in Sect. 2, (5).

Another quite distinct case that is also biologically relevant involves f being linear (Fig. 2(b)). This relates to two different biological scenarios. One of these is that contact with only one surrounding cell is made, and that contact alone determines the outcome of differentiation; such behaviour would be more likely when contact with cells is inhibited, for example due to the presence of Numb as described above. An alternative scenario is that contact occurs with all neighbouring cells, but that the resulting effect on differentiation pathways is linear; this would depend on underlying biochemical details. In either case, the response to the signals produced is linear. We

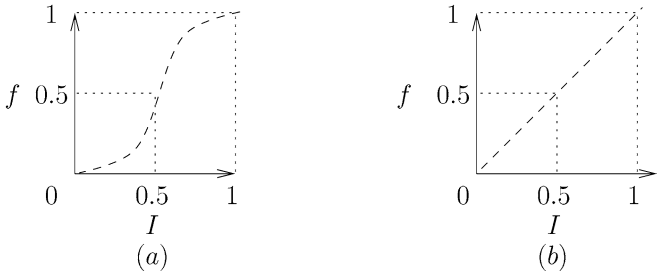

Fig. 2 The *above figure* demonstrates the two chosen f functions for differentiation in our model (7). Figure (**a**) shows a smooth continuous function that is close to a step function. This case represents our community model. Figure (**b**) shows a linear f, which represents our single cell model

call this version the *Single Cell Model*; mathematically it is represented as in (7), but with a linear f.

Note that although our two choices of f for the two local environment models (7) are not comprehensive, with many other reasonable options, f must be monotonic to reflect a community effect as described in Sect. 1, and symmetric in the sense that $f(1/2 - x) + f(1/2 + x) = 1$, $\forall x \in (0, 1/2)$. This symmetry ensures that differentiation is unbiased toward either of the two cell types. Then our two choices of f represent two extremes of this understanding of a community effect and should therefore encompass all types of community effect related behaviour.

We now explore the long term behaviour we can expect from the three models by carrying out some analysis, looking at the location and stability of spatially homogeneous steady states.

3 Analysis of the Three Models

3.1 Analysis of the Autonomous Model

We have that (6) is given by $\frac{da(t)}{dt} = 1/(1 + k) - \alpha_1 a(t)$ and $\frac{db(t)}{dt} = k/(1 + k) - \alpha_2 b(t)$. The only steady state of this simple model is given by $(1/\alpha_1(1+k), (k/\alpha_2(1+k))$, with $k \neq 1$. Noting that this is a system of two uncoupled ordinary differential equations, it is immediately clear that this steady state is globally stable for all positive constants α_1 and α_2. This means that this system will always go to, and remain at, a homogeneous mixing of both cell types, in a proportion that is dictated by the relative rates of differentiation and apoptosis.

3.2 Analysis of the Community Model

Here, the model (7) is given by $\frac{\partial a}{\partial t} = f(I_a) - \alpha_1 a$ and $\frac{\partial b}{\partial t} = f(I_b) - \alpha_2 b$ with all details as in Sect. 2, (5), and f a continuous approximation to a step function as is described in Sect. 2.1.2, and illustrated in Fig. 2(a). The question is what homogeneous steady states are possible, and what combination of stabilities can occur as parameters are varied. Knowing this will allow us to see what are the likely long

term scenarios for the system, and when they might occur. Biologically, this gives us further insight into the type of differentiation dynamics we can expect in real systems.

3.2.1 Sufficient Condition for only Three Steady States

Let $x = a/(a+b)$. Then $1-x = 1-a/(a+b) = b/(a+b)$, and so we have uniform steady states at

$$a = \frac{1}{\alpha_1} f(x) \quad \text{and} \quad b = \frac{1}{\alpha_2} f(1-x). \tag{8}$$

Since $bx = a(1-x)$, (8) implies that $\frac{1}{\alpha_1} f(x)(1-x) = \frac{1}{\alpha_2} f(1-x)x$ at a steady state, i.e. $0 = F(x) \equiv (1-x)f(x) - \gamma x f(1-x)$, where $\gamma = \alpha_1/\alpha_2$. Therefore, there are steady states at $x = 0$ and $x = 1$, corresponding to populations composed entirely of cell type B and cell type A, respectively.[1] Coexistence steady states must satisfy

$$f(x) = \frac{\gamma x}{1 - x + \gamma x}. \tag{9}$$

We now show that for a large class of functional forms of f there is only one solution of (9), i.e. there is only one coexistence steady state.

Proposition *Let f be a smooth, monotonically increasing function, $f : [0,1] \longrightarrow [0,1]$ such that the following hold*:

$$f(x) = 1 - f(1-x), \quad \forall x \in (0,1), \tag{10}$$

$$f(x) = x \quad \text{for } x = 0, \frac{1}{2}, 1; \qquad f(x) \neq x \quad \text{otherwise}, \tag{11}$$

$$f'(x) = 0 \quad \text{for } x = 0, 1; \qquad f'(x) \neq 0 \quad \text{otherwise}, \tag{12}$$

$$\begin{aligned} f''(x) &> 16\gamma(1-\gamma)/(\gamma+1)^3, \quad \forall x \in \left(0, \frac{1}{2}\right) \text{ when } \gamma \in (0,1), \\ f''(x) &< 16\gamma(1-\gamma)/(\gamma+1)^3, \quad \forall x \in \left(\frac{1}{2}, 1\right) \text{ when } \gamma > 1. \end{aligned} \tag{13}$$

Then (7) have exactly three steady state solutions.

Note that these conditions are sufficient but not necessary. Mathematically, the restriction on the size of f'' prevents multiple steady states on $(0,1)$ by limiting the curvature of f.

Proof Let $\gamma \in (0,1)$. We begin by defining $g(x) = \gamma x/(1 - x + \gamma x)$; then (9) implies that steady states satisfy $f(x) = g(x)$. Trivially, $f(0) = g(0) = 0$ and $f(1) = g(1) = 1$, giving us our first two solutions. We now just need to prove the uniqueness of solutions on $(0,1)$ under the above conditions.

[1] Note that the trivial case $(0,0)$ is also a steady state.

We have that $g'(0) = \gamma > f'(0)$, and $g'(1) = \frac{1}{\gamma} > f'(1)$. Therefore, $f(x) = g(x)$ must have at least one solution with $x \in (0, 1)$. Suppose first that $\gamma \in (0, 1)$. Then straightforward calculation shows that $g(x) < x, \forall x \in (0, 1)$, while (11) and (12) imply that $f(x) \geq x, \forall x \in [\frac{1}{2}, 1)$. Therefore, there are no solutions of (9) on $[\frac{1}{2}, 1)$. Moreover, (13) implies that $f''(x) > g''(1/2) > g''(x), \forall x \in (0, \frac{1}{2})$. This ensures that $g(x)$ does not meet $f(x)$ more than once for $x \in (0, \frac{1}{2})$ giving us exactly one more solution to $f(x) = g(x)$ as required. The proof is similar in the $\gamma > 1$ case. Note that for $\gamma = 1$ the case is trivial, as here $g(x) = x$, and so by (11) there are only three steady states. □

3.2.2 Stabilities of Steady States

Calculation of the stability matrix of (7) shows that the single species steady states are both stable. We now show that when there are just three homogeneous steady states of the community model (7), where f satisfies conditions (10)–(13), the (unique) coexistence steady state is unstable. Define $F(x) = (1 - x)f(x) - \gamma x f(1 - x)$ as before. Then by (10),

$$F'(x) = f(x)(\gamma - 1) + f'(x)(1 - x - \gamma x) - \gamma. \tag{14}$$

Then assuming (11) and (12) hold, $F'(0) = -\gamma < 0$ and $F'(1) = -1 < 0$ by direct substitution into (14). Therefore, by continuity, there must be a point $x^* \in (0, 1)$ with $F(x^*) = 0$ and through which F increases with x. Since we assume only three steady states, this must be the unique coexistence steady state. We now calculate the stability matrix of the spatially uniform version of (7). The equations in question are $\frac{\partial a}{\partial t} = f(x) - \alpha_1 a$ and $\frac{\partial b}{\partial t} = f(x) - \alpha_2 b$. The stability matrix is then

$$\begin{pmatrix} f'(x)b(a+b)^{-2} - \alpha_1 & -f'(x)a(a+b)^{-2} \\ -f'(1-x)b(a+b)^{-2} & f'(1-x)a(a+b)^{-2} - \alpha_2 \end{pmatrix},$$

and the determinant is given by

$$-\alpha_2/(a+b)\big(f'(x)(1-x) + \gamma x f'(1-x) - \alpha_1(a+b)\big).$$

Since at the steady states, $f(x) = \alpha_1$ and $f(1 - x) = \alpha_2$, straightforward calculation shows that the determinant is $-\alpha_2 F'(x)/(a + b)$. Therefore if $F'(x^*) > 0$, the steady state is unstable, so that the only stable homogeneous states consist of populations composed of only one of the cell types. We have not attempted an investigation of the behaviour when $F'(x^*) = 0$, which would require a calculation of the centre manifold of the ODE system, but our expectation is that the coexistence steady state will always be unstable in this case also.

3.3 Analysis of the Single Cell Model

This model (7) is again given by $\frac{\partial a}{\partial t} = f(I_a) - \alpha_1 a$ and $\frac{\partial b}{\partial t} = f(I_b) - \alpha_2 b$, with f linear as discussed in Sect. 2.1.2 and illustrated in Fig. 2(b). The number of spatially uniform steady states in the single cell model varies according to whether the death rate parameters are equal or not, so we investigate the two cases separately.

3.3.1 Case 1: $\alpha_1 = \alpha_2$

If $\alpha_1 = \alpha_2 = 1/c$, say, this model has a continuum of non-trivial spatially uniform steady states at $(a, b) = (a_s, c - a_s)$, $0 \leq a_s \leq c$. Linear analysis shows that these steady states exhibit neutral stability. This means that we expect the system to remain at whatever population density of each cell type it began with. This is of particular interest biologically, as it suggests that in this case, there will be a persistence of both cell types over time. This also occurred in the autonomous model, but is in marked contrast to the behaviour seen in the community model.

We now explore what happens if, when $\alpha_1 = \alpha_2 = 1/c$, $a + b \neq c$ initially. Then we do not begin along the line of neutral stability—our populations must move onto it. To investigate this, we consider the case of two spatially homogeneous cell populations. We have

$$\frac{da}{dt} = a\big[1/(a+b) - 1/c\big], \tag{15a}$$

$$\frac{db}{dt} = b\big[1/(a+b) - 1/c\big] \tag{15b}$$

by simple rearrangement of the spatially homogeneous version of (7), with $c = 1/\alpha_1 = 1/\alpha_2$ as stated above. Combining (15a) and (15b) gives $da/dt = (a/b).(db/dt)$, which leads to

$$a = b/\Gamma \tag{16}$$

where Γ is a constant of integration. Equation (16) can then be substituted back into (15a) to give a single equation for $a(t)$ only:

$$\frac{da}{dt} = a\big[1/(a + \Gamma a) - 1/c\big]. \tag{17}$$

Since Γ is constant, it can be found by looking at the initial values of a and b, i.e.

$$\Gamma = b_0/a_0, \tag{18}$$

where a_0 and b_0 are our initial conditions. Substituting (18) into (8) and (17) implies that a steady state with $a > 0$ must satisfy

$$a = ca_0/(a_0 + b_0), \qquad b = cb_0/(a_0 + b_0). \tag{19}$$

By looking at (17), we can further show that this solution is globally stable: if a is larger than our positive solution given by (19), then $\frac{da}{dt} < 0$, while if a is smaller, $\frac{da}{dt} > 0$.

3.3.2 Case 2: $\alpha_1 \neq \alpha_2$

For this scenario, we have only the steady states $(a, b) = (\frac{1}{\alpha_1}, 0), (0, \frac{1}{\alpha_2})$, i.e. there is no coexistence steady state. This suggests that in this case, the system will always evolve to a single species steady state, suggesting dynamics that will be different to the autonomous model, but which may have some agreement with the community model.

Table 1 A summary of stability of the steady states of the three models

Model type	Steady state	Type	Stability
Community	$(\frac{1}{\alpha_1}, 0)$ or $(0, \frac{1}{\alpha_2})$	Single species	Stable
	(a_s, b_s)	Coexistence	Unstable
Autonomous	$(1/\alpha_1(k+1), k/\alpha_2(k+1))$	Coexistence	Stable
Single cell	$(a_s, b_s) \in [0, c]$, $c = 1/\alpha_1 = 1/\alpha_2$ if $\alpha_1 = \alpha_2$	Coexistence	Neutral
	$(\frac{1}{\alpha_1}, 0)$ or $(0, \frac{1}{\alpha_2})$ if $\alpha_1 \neq \alpha_2$	Single species	Stable

3.4 Summary

This analysis of the three variations of our model has shown that the way in which differentiation is regulated by the contact between precursor cells and their local environment significantly alters the balance of cell types we can expect to see, as summarised in Table 1. This analysis of steady states and their stability provides a firm foundation for the numerical analysis of the spatiotemporal dynamics that develop from different initial conditions.

4 Numerical Analysis of the Three Models

While the linear analysis provides some insight into the expected model behaviour, we carry out a numerical study for further understanding. We first consider a one-dimensional version of the model, using a simple numerical scheme that discretises the line integral through space, summing the integral over each point and averaging over the length. Similarly, our two-dimensional numerical code discretises the circular domain of the integral, and then sums the integral over each of the grid squares within the circle. Although some of the area of the circle is lost at the boundaries, the calculation is fast and, with a fine lattice, it is reasonably accurate; in particular, when we reduce our lattice in size by a factor of two, our results are qualitatively the same. For the two-dimensional case, more sophisticated numerical schemes for integro-differential equations using techniques such as fast Fourier transforms to evaluate the integral are possible: see in particular Gerisch and Chaplain (2008) and Gerisch (2010). To solve the resulting system of ODEs, we use a fast and straightforward Euler method in the simple one dimensional case, while in the more complicated two dimensional case, we use ROWMAP (Weiner et al. 1997), a method that is particularly suited to solving stiff ODE initial value problems, and which automatically controls and adjusts time-step size.

4.1 The One-Dimensional Model Results

We begin by investigating a homogeneous mix of cell populations with noise in order to explore the patterns created from a randomly mixed group of cells. Such random mixing is seen, for example in the regeneration of ablated pigment cells in experiments on zebrafish, suggesting that pigment precursor cells in the zebrafish are distributed randomly (Yamaguchi et al. 2007). We investigate the autonomous, community, and single cell models in turn.

4.1.1 The Autonomous Model

First, we look at the autonomous model (6). For all α_1's and α_2's, the system moves quickly to the steady state $(1/\alpha_1(k+1), k/\alpha_2(k+1))$, $k \neq 1$ as expected (not shown). The initial noise rapidly disappears, leaving solutions that are homogeneous across the domain, demonstrating that the system does not produce patterning.

4.1.2 The Community Model

We now consider the community model (7) with f as in Fig. 2(a). We see that here, stripes sometimes develop from the random initial conditions, although they are transient unless $\alpha_1 = \alpha_2$—this case is special as only here is the model balanced and bistable (i.e. there is a symmetry between the basins of attraction of the two stable steady states). Clearly, stripe formation is not robust, as it is not always seen even if $\alpha_1 = \alpha_2$; also, while stripes persist for longer as α_1 approaches α_2, they are permanent only if the death rates of the two cell populations are equal (Fig. 3). The width of the stripes is dependent on the length of the sensing radius used (Fig. 4, upper panel). This is as expected, since on an infinite domain, changing the sensing radius is equivalent to rescaling space. Obviously, both the timescale and the stripe width of interest depends on the biological system we are investigating; we discuss this for the specific case of pigmentation stripes on zebrafish in Sect. 5.

Finally, simulations with initial conditions consisting of stripes perturbed by a small amount of random noise indicate that the permanent stripes of the $\alpha_1 = \alpha_2$ case are stable to small perturbations (Fig. 4, lower panel), while when $\alpha_1 \neq \alpha_2$, this is not the case even for α_1 close to α_2 (not shown). This has relevance to the concept of stripe maintenance, which we again discuss in detail in the context of the zebrafish example in Sect. 5.

4.1.3 The Single Cell Model

We complete our one dimensional study by considering the single cell model (7), with f as in Fig. 2(b). When $\alpha_1 \neq \alpha_2$, the system evolves to a homogeneous steady state as suggested by the analysis in Sect. 3.3.2 (not shown). However, when $\alpha_1 = \alpha_2$, we see a mix of both cell lines homogeneously across the domain, as suggested by the results in Sect. 3.3.1, with the long-term steady state being as predicted by (19) (Fig. 5). Despite this difference in behaviour between the cases $\alpha_1 \neq \alpha_2$ and $\alpha_1 = \alpha_2$, the key implication is the same in both: we do not see patterning. Therefore, only one of our three model types produces spatial patterns in one dimension: the community model, with $\alpha_1 = \alpha_2$ a necessary condition for permanent, stable patterns in that case.

We will now go on to investigate simulations on a two-dimensional domain, in order to more effectively explore the spatial aspects of the models.

4.2 The Two-Dimensional Model Results

We again begin by investigating a homogeneous mix of cell populations with a small amount of noise, for reasons discussed in Sect. 4.1.

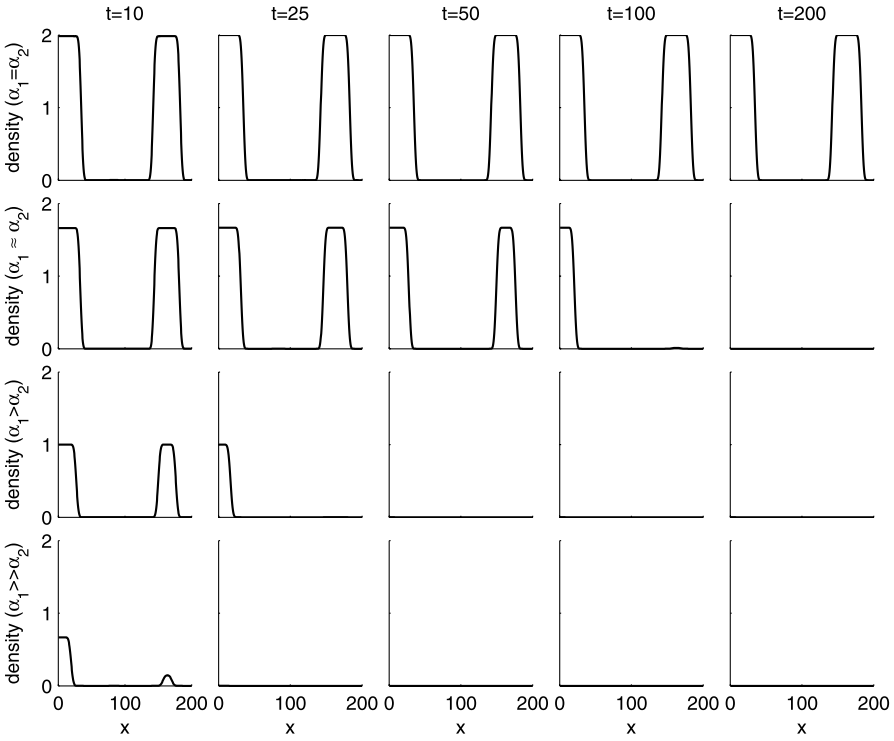

Fig. 3 Solutions of the community model (7) with f as in Fig. 2(a), in one dimension. We begin from random initial conditions. We plot the density of cell type A through space at dimensionless times indicated, and vary the death rates (note that the density of B is omitted for clarity). The death rate $\alpha_2 = 0.5$ in all four cases, with $\alpha_1 = 0.5, 0.6, 1.0, 1.5$ (from the *upper panel* down). When the death rates of the two populations are equal (*upper panel*), stripes develop about 70% of the time (706 out of 1000 runs produced stripes that persisted for long simulation times). However, unequal death rates always eventually produce dominance of a single species across the domain, with the time taken for one species to dominate decreasing as the difference between the two death rates increases. Note that despite their piecewise linear appearance at this magnification scale, the solutions are in fact smooth. All other numerical details are as described in Sect. 4. Initially, random values between 0 and 0.02 are chosen for a and b at each numerical grid point, from a uniform distribution. The domain is of length 200 dimensionless space units. The function f is given by $f(I) = 0.5\tanh(\tan(I\pi - 0.5\pi)) + 0.5$, a continuous approximation to a step function. The dimensionless parameter value $R = 10$. The space discretisation is $\Delta x = 0.5$, and the time discretisation is $\Delta t = 0.01$

4.2.1 The Autonomous Model

In this model, we see each cell population evolving to the steady state suggested in Sect. 3.1, spread homogeneously across the domain (not shown). These states are stable over time, and show that cell autonomous differentiation results in the persistence of both cell types. For our zebrafish example, this suggests that autonomous differentiation can not be the sole process behind the differentiation of chromatophore precursors, since such a mode of differentiation will always fail to produce patterning.

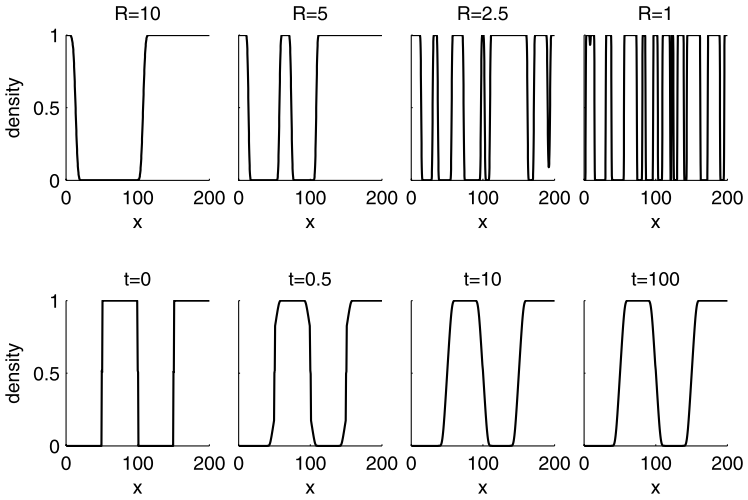

Fig. 4 *Upper panel*: Solutions of the community model (7) with f as in Fig. 2(a) in one dimension at time $t = 10$, demonstrating that different sizes of sensing radii produce differently sized stripes. We set $\alpha_1 = \alpha_2 = 1$, and adjust R as indicated. We see that decreasing R produces a decrease in stripe width. We set $\Delta x = 0.2$. All other numerical details are as in Fig. 3. *Lower panel*: A solution of the community model (7) with f as in Fig. 2(a) in one dimension at times $t = 0$, $t = 0.5$, $t = 10$ and $t = 100$, with initial conditions of stripes, perturbed by random noise. This shows that stripes are stable over time. The initial conditions are $a = 0.0$ for $x \in (0, 49.5)$ and $x \in (100.5, 149.5)$, $a = 1$ for $x \in (50.5, 99.5)$ and $x \in (150.5, 200)$, and $a = 0.5 + n_1/50$, $b = 0.5 + n_2/50$ for $x \in (49.5, 50.5)$, $x \in (99.5, 100.5)$ and $x \in (149.5, 150.5)$, where both n_1 and n_2 are random numbers between 0 and 1, chosen from a uniform distribution, calculated at each numerical grid point. We set $\alpha_1 = \alpha_2 = 1$, with all other numerical details as in Fig. 3

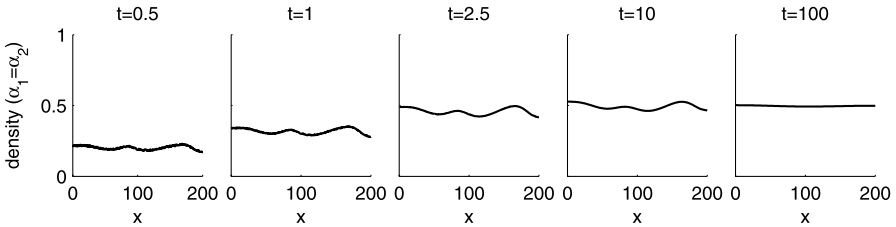

Fig. 5 Solutions of the single cell model (7) with f as in Fig. 2(b) in one dimension, beginning from random initial conditions, and with equal death rates. We again plot the density of cell type A through space at dimensionless times indicated. We see that the system evolves to a homogeneous steady state, as expected from (19) and the analysis of Sect. 3.3.1. In 1000 simulations, we never saw stripes. We set $f(I) = I$ and $\alpha_1 = \alpha_2 = 1$, with all other numerical details as in Fig. 3

4.2.2 The Community Model

We look at two separate cases, as suggested by our one-dimensional results in Sect. 4.1.2. We first consider the case where $\alpha_1 \neq \alpha_2$, i.e. the death rates of the two cell populations are distinct. We ran simulations with a variety of different $\alpha_1 \neq \alpha_2$ pairs, and a variety of different seeds for the noise in the initial conditions, for

a 10×10 domain. In this case, the system always moves rapidly to a steady state, at which only the cell type with the smaller death rate is present, even when α_1 is close to α_2 (including, for example, $\alpha_1 = 0.99, \alpha_2 = 1.01$). In contrast to the one-dimensional case, where transient stripes form when death rates are sufficiently close, here patterning is not seen across the domain. This could be to do with the size of our domain as well as the death rates, since the time-consuming nature of the simulations requires us to use a domain that is too small to show stripes of the wavenumber seen in the one-dimensional simulations in Sect. 4.1.2. Note that in a one-dimensional simulation on a domain of length 10 (which is the side-length of our two-dimensional domain) with equal death rates, we do not see multiple stripes as in Fig. 3, but rather a single stripe (not shown). We discuss this in more detail below.

We now turn to the case $\alpha_1 = \alpha_2$. The death rates are then the same for the two populations, suggesting that they are of very similar type. Again we consider only a 10×10 square spatial domain. The system moves directly to a single species steady state in 15 out of 20 runs, and to a split domain in the other 5 runs (see Fig. 6),

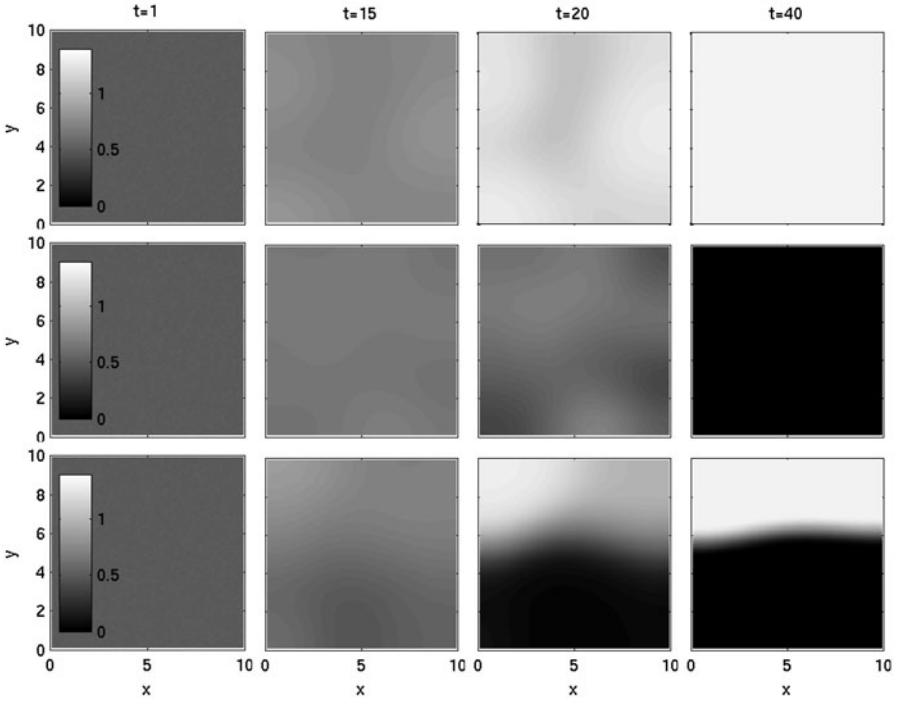

Fig. 6 A solution to the community model (7) with f as in Fig. 2(a) and with random initial conditions as described below. All numerical details are as described in Sect. 4. We plot the proportion of cells of type A in space at dimensionless times $t = 1$, $t = 15$, $t = 20$ and $t = 40$. The *upper two panels* show dominance of a single species across the grid. The *lower panel* shows dominance by neither cell type, which held for long times (solutions were found to be stable in runs up to $t = 10^8$; not shown). Out of 20 runs, A dominated 7 times, B 8, and neither 5. We begin with initial conditions of $a = 0.5 + 0.02 \times n$ where n is chosen randomly between 0 and 1 from a uniform distribution at each numerical grid point. The dimensionless parameter values are $R = 1.0$, $\alpha_1 = \alpha_2 = 0.75$. The domain is of length 10 dimensionless space units. We set the absolute error tolerance in the ROWMAP scheme to 10^{-6}

showing the capability of the model to produce distinct boundaries between the two populations, in a manner consistent with the formation of stripes. The proportion 5/20 is much lower than that in the one-dimensional case, which saw full stripes in 70% of cases. As mentioned above, this difference in proportions makes sense, since the one-dimensional geometry encourages stripes and, moreover, the domain is sufficiently long to see stripes of various wavenumbers. In contrast, the two-dimensional 10×10 domain is too small to see such complete stripes form. The improved computational method for the integral described by Gerisch (2010) would greatly facilitate us in a search for stripes in two dimensions, and implementation of this is a natural area for future work. In cases where we do not see a split domain, the final single species steady state is dependent on the initial conditions, with whichever cell type has the greater initial density being dominant.

4.2.3 The Single Cell Model

Again, we first consider the case $\alpha_1 \neq \alpha_2$, i.e. the death rates for the two populations are distinct. As in the community model, the system goes to a single species steady state, as suggested by our stability analysis in Sect. 3.3.2 (not shown). It is again the cell type with the smaller death rate to which the system evolves.

Next, we let $\alpha_1 = \alpha_2 = 1/c$, where c is a constant as in Sect. 3.3.1. Here, stability analysis suggests that we will see a merging of the two initial populations into one spatially uniform population spread across the domain, with the two individual cell types being in the same proportion as they were at the beginning of the simulation, although now spread homogeneously. This is indeed what we see (Fig. 7). This behaviour contrasts with that in the community model, but is similar to the results of our

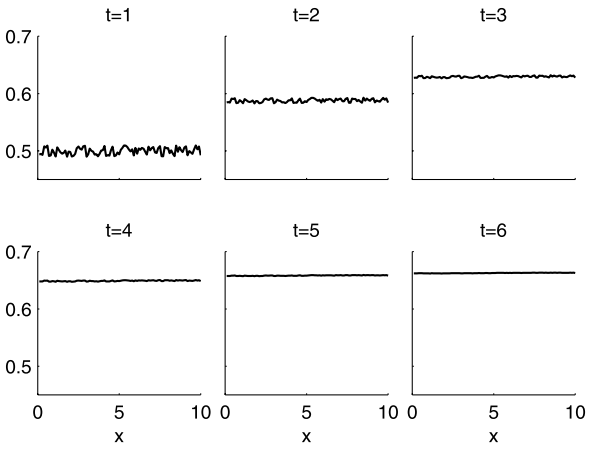

Fig. 7 Time evolution plots of the two dimensional single cell model (7). The domain is initially an even mix of the cell populations A and B, as described in Fig. 6. We plot the density of cell type A across space in the x direction for $y = 2$ at various times t, until $t = 6$. We see the density of A increasing quickly, with the spatial variation in the initial density rapidly smoothing out, and with the density of A approaching 2/3 everywhere, as expected from (19). All parameter values and numerical details are as in Fig. 6, although with $f = I$ as stipulated by this model (see Fig. 2(b))

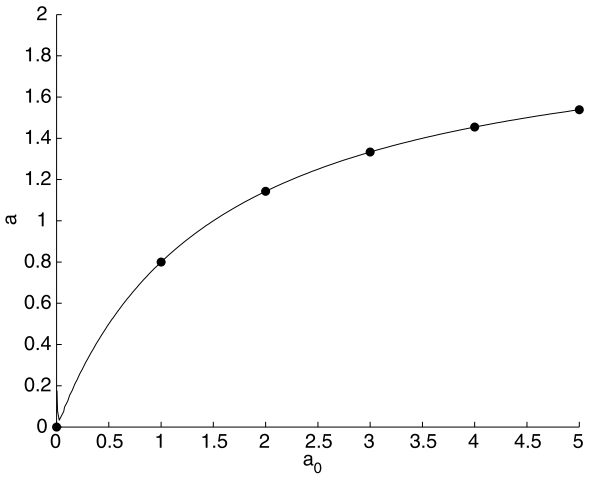

Fig. 8 The *solid line* shows the solution to (19) with $c = 2$, so that $\alpha_1 = \alpha_2 = 1/2$ and $b_0 = 1.5$. Equation (19) gives estimated steady state values in the solution of (7) for a when $a + b \neq c$ initially. We fix $b_0 = 1.5$, and plot the steady state a as a function of a_0, where both $b = b_0$ and $a = a_0$ initially. Spots indicate the actual numerical steady state values of (7) given by the initial conditions indicated. Note the near identical match between the integro-differential equation and ODE solutions. In the numerical simulations of (7), initial conditions are set to $b = 1.5$ across the domain, and $a = a_0 + 0.02 \times n$, where n is chosen randomly from a uniform distribution between 0 and 1 at each numerical grid point and values of a_0 chosen are 0, 1, 2, 3, 4, and 5. All other parameter values and numerical details are as in Fig. 7

autonomous model. When $a + b \neq c$ initially, the two cell types go to the densities suggested in Sect. 3.3.1, (19) (Fig. 8).

4.3 Extending the Two-Dimensional Model Results

We now consider three other initial conditions, in order to further explore some of the behaviours discussed above. In Sect. 4.2.2, the community model in the case $\alpha_1 = \alpha_2$ sometimes resulted in a split domain with different cell types present in the two parts. In order to investigate this phenomenon further, we repeat our experiments, this time starting with split conditions similar to those seen in the lower panel of Fig. 6 at time $t = 40$. With these split initial conditions, the interface between the two species does not move over long times, suggesting that we are indeed at a steady state (not shown). Furthermore, we repeat our experiments with a curved interface (see Fig. 9) in order to discover whether the speed of propagation depends on curvature. We observe a flattening of the interface (Fig. 9), but no further movement. This coincides with the previous result, and suggests that a coexistence steady state in the community model will typically display a flat interface between the two species.

Finally, we investigate "island" initial conditions (see Fig. 10, first column), in order to explore the dynamics of a localised group of cells. As in the previous result, we find that movement is fastest where curvature is greatest, with the motion roughly proportional to the mean curvature of the wavefront. This leads to the "island" shrinking until it disappears in nearly all cases (see Fig. 10, upper panel), explaining both why we sometimes see the dominance of a single species in the community model,

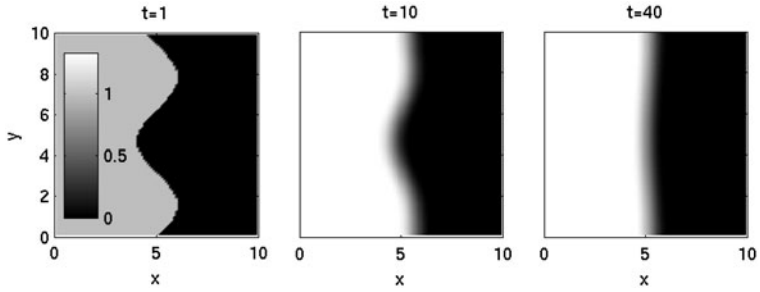

Fig. 9 Solutions to the two-dimensional community model (7) with curved initial conditions. We plot the density of B cells in space at $t = 1$, $t = 10$, and $t = 40$. Neither cell type dominates over long times. All numerical details and parameter values are as in Fig. 6

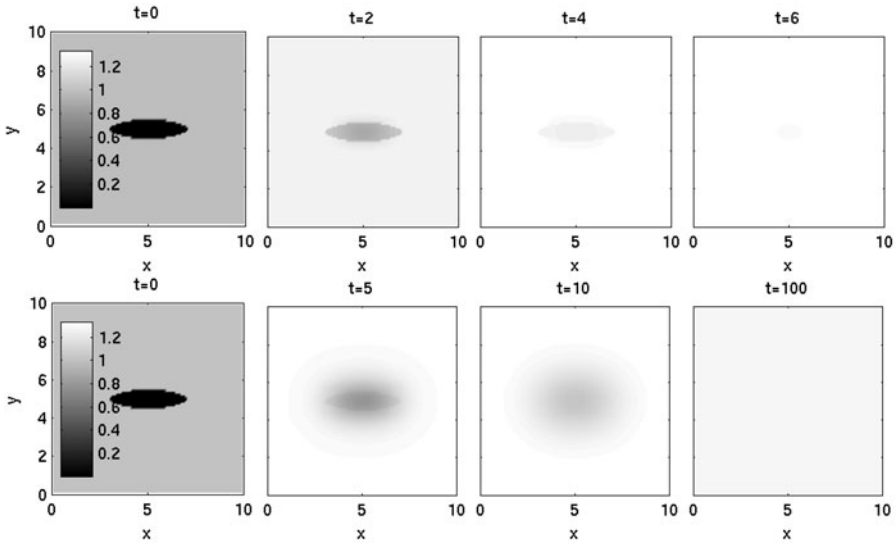

Fig. 10 Solution of both the two-dimensional community model and single cell model (7) with island initial conditions. The domain is initially split with type A the "sea", and B the "island". We plot the density of cell type A in space at the dimensionless times indicated. Community model (*upper panel*): A dominates across the domain. The dimensionless parameter values are $\alpha_1 = 0.75$, $\alpha_2 = 1.5$. All other parameter values and numerical details are as in Fig. 6. Single cell model (*lower panel*): With equal death rates, the initially localised population of cell type B spreads across the domain, merging with the population of cell type A and eventually becoming homogeneous. The dimensionless parameter values are $\alpha_1 = 0.75 = \alpha_2$. All other parameter values and numerical details are as in Fig. 6, although with a different f as stipulated by this model

and why we do not see stable spotted patterns, as each small group of cells is engulfed by the larger local population. However, if the death rate of the "island" is sufficiently small in comparison to the death rate of the other cell population, then an "island" will grow and dominate the domain (see Fig. 11 for details of this for circular islands).

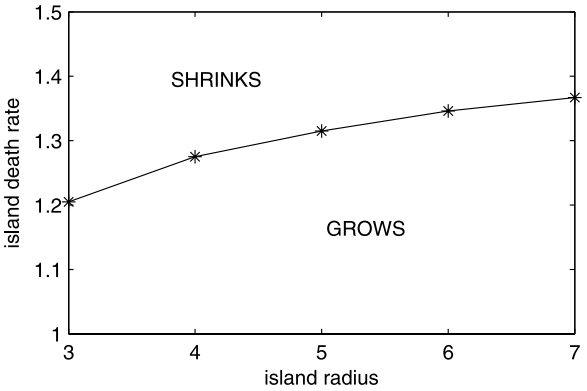

Fig. 11 Plot of island radius versus death rate for a circular island, showing the parameter regions in which the island will shrink or grow. We set the second cell population to have a death rate of 1.5. We see that as the island increases in size, a higher death rate of the island cell population is required in order for the island to shrink. Critical values were calculated by reducing the problem to one dimension, making use of the circular symmetry; this makes numerical solutions very much faster than the corresponding two-dimensional simulations—see the Appendix for more details. Initially, random values between 0 and 0.02 are chosen for a from a uniform distribution at each numerical grid point if $x \leq$ the island radius being investigated, while $b = 1 - a$. The island radii chosen are $R = 3$, 4, 5, 6 and 7. Various death rates for the island population are investigated in order to find the critical value to 4 significant figures. The domain is of length 100 dimensionless space units, the dimensionless parameter value $R = 1$, and the space discretisation is $\Delta x = 0.1$. All other numerical details are as in Fig. 3

We now consider the same "island" initial conditions for the single cell model in order to see how a small group of cells evolves over time under this differentiation rule. When $\alpha_1 \neq \alpha_2$, we find a direct relationship between the death rates of the two populations and the final steady state for all sizes of "island", with the population with the smaller death rate dominating across the domain, and having a density of either $a = 1/\alpha_1$ or $b = 1/\alpha_2$ (not shown). However, when $\alpha_1 = \alpha_2$, our analysis in Sect. 3.3 suggests we will see a merging of the two cell populations across the domain, as is seen in Fig. 7. This is indeed what we find in our simulations, with the overall ratio of cell densities remaining constant (Fig. 10, lower panel). From a biological viewpoint, this suggests that even a small initial population of cells will persist over time under this differentiation scenario.

4.4 Summary of Two-Dimensional Results

These results suggest that only the community model (7), which represents a strong community effect, has the ability to generate spatial patterns consisting of two distinct groups of cells through differentiation alone. These stripes exist permanently only if the death rates of the two cell populations are equal. The requirement of a non-linear function f means that patterning requires a markedly non-linear response to the local environment, i.e. we need our function f to be of the form shown in Fig. 2(a) rather than that shown in Fig. 2(b). Without this non-linear response, no patterns will be seen for any death rates. One simple implication of this result is that a community effect may be in play in scenarios where we do not see patterning.

5 Discussion

Our results demonstrate that patterning can only be obtained in the model via a non-linear response to the local environment: the fate of a differentiating cell must be strongly biased by the ratio of cell types in its local environment. This is the only way to achieve patterning through a local environment-dependent differentiation process alone; the community model, which follows this non-linear process, does produce patterns in some cases, but neither the cell autonomous or the single cell model do. Even with a strong effect, the formation of stripes depends on initial conditions and is therefore not robust: a small bias toward stripe formation in the initial conditions is required for stripes to form. We also note that, significantly, for permanent stripes to form it is necessary that the two death rates are equal. However, transient stripes are seen for distinct death rates (see Fig. 3 and Sect. 4.1.2). This shows that on a short timescale, a community effect can produce patterns with unequal death rates. Obviously, the timescale of interest varies according to the biological system being investigated, and we discuss timescales in relation to the zebrafish example below.

In investigating the relevance of the model to zebrafish stripe formation, we first consider the width of the stripes seen in our simulations; these should match realistic zebrafish stripe widths if our model is to be relevant. The typical width of a melanophore stripe is 6 cells, while a xanthophore stripe is typically wider once fully formed (Moreira and Deutsch 2005). If we assume that the sensing radius of a cell is equal to its physical radius, then the stripes formed in Fig. 3 are not sufficiently wide to be realistic melanophore stripes. Therefore, although our system is clearly able to produce patterning for other systems which contain narrower stripes, we conclude that a community effect is insufficient in itself as a mechanism for creating stripes and other patterns in zebrafish; permanent and accurate stripe formation requires coupling with a stronger mechanism such as homotypic cellular attraction (Caicedo-Carvajal and Shinbrot 2008; Maderspacher and Nusslein-Volhard 2003), intercellular adhesion (Moreira and Deutsch 2005), or indeed, perhaps something entirely different such as a reaction-diffusion system (see Kondo et al. 2009 for a review).

We now look to see whether a strong community effect is sufficient for stripe maintenance in zebrafish. We begin our simulation on a rectangular domain with a central stripe running parallel to the long edge. Over long times, the stripe remains if $\alpha_1 = \alpha_2$ (not shown), and widens or shrinks if the two death rates vary (Fig. 12). To make our observations specific to zebrafish, we carry out further simulations again with a realistic stripe width, fixed in comparison to the sensing radius: we again assume that the sensing radius of a cell is equal to its physical radius, and impose stripe widths of 6 cells for melanophores and 9 cells for xanthophores (Moreira and Deutsch 2005). These stripes are wider than those formed transiently in Fig. 3. We now define maintenance to occur if the stripe width changes by less than 25%, with a density of no less than 75% of the original stripe density. With the stripe initial conditions stated, we vary the death rates and find that for various values we see stripe maintenance over a finite period of time.

In order to understand the extent to which these transient dynamics are relevant to zebrafish pigmentation patterns, we estimate the dimensional time over which patterns develop, as implied by the model (7). Note that this means the dimensional

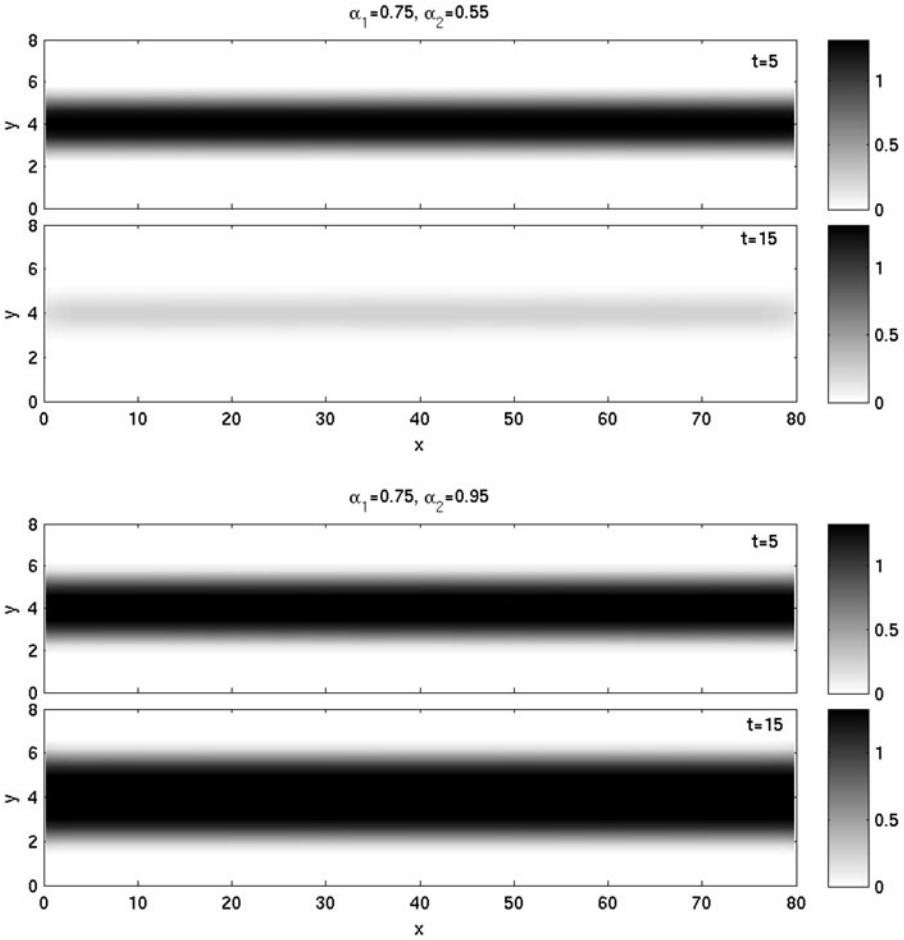

Fig. 12 A simulation of stripe maintenance. We plot the density of A at the time points indicated. We begin with a striped domain, and see the stripe alter over time. When the death rate of A is greater than that of B, the stripe width decreases (*top two panels*), while stripe width increase is seen in the converse case (*lower two panels*). We see that the system is able to maintain stripes for a finite period of time. Note that the stripe width and density do not change over time when death rates are equal (not shown). We use $\alpha_1 = 0.75$, $\alpha_2 = 0.55$ in the *upper panel*, and $\alpha_1 = 0.75$, $\alpha_2 = 0.95$ in the *lower panel*. The initial conditions are $a = 1$, $b = 0.02 \times n$ for $y \in [3, 5]$, $a = 0.02 \times n$, $b = 1$ otherwise, where n is a random number chosen from a uniform distribution $\in (0, 1)$ generated at each point. The domain is of size 8×80 dimensionless space points. All other details are as in Fig. 6

half-life value is implicitly related to the dimensional death rate of the cells. As a somewhat arbitrary estimate for the half-life of a zebrafish melanophore (population A in our model, say), we use 5 days, so that

$$\ln 2/\alpha_1 \times P/\tilde{\alpha}_0 p = 5 \text{ days},$$

following the non-dimensionalisation in Sect. 2. In Fig. 3, say, we used a dimensionless melanophore death rate of $\alpha_1 = 1$ in the third panel, and see two stripes at

Table 2 Simulation results on the ability of the community model (7) to maintain stripes; the function f is as in Fig. 2(a). We fix our melanohphore half-life, and vary our xanthophore half-life by the percentages shown. We see that a stripe is maintained over the course of a year for a wide variety of half-lives. We set the melanophore death rate at $\alpha_1 = 0.75$ and, from left to right, we set $\alpha_2 = 0.68, 0.83, 0.63, 0.94, 0.58, 1.07$. The initial conditions for the one-dimensional simulations used for this table are $a = 1$, $b = 0 + 0.02 \times n$ for $x \in [18, 30]$, $a = 0 + 0.02 \times n$, $b = 0$ otherwise, where n is a random number chosen from a uniform distribution $\in (0, 1)$ generated at each point. The domain is of size 48 dimensionless space points. All other details are as in Fig. 3

Do we see stripes maintained after one year?						
melanophore half-life \ xanthophore half-life (% of m.h.-l.)	10%		20%		30%	
	+	−	+	−	+	−
25 days	Yes	Yes	Yes	Yes	Yes	Yes
5 days	Yes	Yes	Yes	Yes	Yes	No
2.5 days	Yes	Yes	No	No	No	No
1 day	No	No	No	No	No	No

dimensionless $t = 10$. The corresponding dimensional time is then

$$10 \times P/\tilde{\alpha}_0 p = 10 \times 1/\ln 2 \times 5 \text{ days} \approx 72 \text{ days}.$$

In the absence of data on the half-life of a melanophore, we present the results for different possible values (Table 2). If the half-life of a melanophore is 5 days, then stripes are maintained for at least 1 year even if the half-life of the xanthophores is 30% more than that of melanophores, or 20% less. The asymmetry between increased and decreased half-lives is due to the absolute difference in values of the associated death rates of the two populations. Whilst this difference is present in all cases, it is greatest in this 30% variation case. Here, while in the +30% case the death rate of xanthophores is 0.17 less than that of melanophores, in the −30% case it is 0.32 greater than that of melanophores, leading to the fast spreading of the melanophore stripe and hence a lack of stripe maintenance. If we decrease the half-life of melanophores to 2.5 days, stripes are still maintained for at least one year when the difference between the half-lives of the two populations is 10%, showing that stripes are maintained under the community model over a wide range of half-lives. Therefore, although we do not know exact half-life values, we conclude that a strong community effect is plausible as a mechanism for stripe maintenance in zebrafish. A possible future extension would

be to explore the capacity of the model to replicate pattern regeneration following experimental ablation of the pigmentation stripes (Rawls and Johnson 2000; Yamaguchi et al. 2007).

We now move away from the zebrafish example, and return to more general implications of our model. We began our model construction in Sect. 2 by assuming that stem cells produce precursor cells at a constant rate, and also self-renew as they do so. However, another possible outcome of stem cell mitosis is the production of two precursors, and no stem cells, or two stem cells and no precursors (see Watt et al. 2006, for a discussion of this in the epidermis). One could model both of these scenarios and see what effect they had on the final outcome of the model, and since so little is known about stem cells and precursor cells in many systems, the mathematical modelling of such scenarios would provide insight into plausible possibilities for different systems. Note also that our two choices of f for the two local environment models are not comprehensive, and there are many other options that one may consider. Further work could reconsider our interpretation of a community effect (Sect. 2.1.2) to see how our results would be affected by a different f.

Further note that in the model we use an integral term to measure the density of cell types in the local environment, and hence to calculate which cell type is in the majority. This calculation depends on the size of the sensing radius R, representing the effective reach of cells. This means that through varying the size of R we could examine the effects of different sensing methods on the model results, and so consider both direct cell-cell contact generated 'decision making' such as that mediated by juxtacrine signalling (small R), and also chemical-based methods such as quorum sensing in bacteria (Atkinson and Williams 2009), where we can make R larger to suggest a diffusive chemical. In this second scenario, the presence of more cells of one type is directly associated with more inductive chemicals of that type. We would use our non-linear function f as in Fig. 2(a) to describe the threshold level of chemical necessary for a change in bacterial activity to take place.

The model (5) could be further extended and altered to look at various other phenomena in which a community effect may be implicated. For example, we could use it to explore Gurdon's work on myogenesis in *Xenopus* (Gurdon 1988; Gurdon et al. 1993a). In these experiments, Gurdon took a small collection of undifferentiated animal cells and observed them collectively differentiating into muscle. Gurdon hypothesised that fully differentiated cells have no effect on the differentiating cells, but rather the cells differentiate when the number of undifferentiated cells reaches a threshold value. Denoting undifferentiated precursors by P, differentiating cells by A, differentiated cells by $\tilde{A}$, a suitable model would be

$$\begin{aligned}
\frac{\partial p}{\partial t} &= -kpf(I_p),\\
\frac{\partial a}{\partial t} &= kpf(I_p) - \alpha a,\\
I_p &= \frac{1}{\pi R^2}\int_0^R\int_0^{2\pi} \frac{p(\underline{x}+r\underline{\eta})}{a(\underline{x}+r\underline{\eta}) + p(\underline{x}+r\underline{\eta}) + \tilde{a}(\underline{x}+r\underline{\eta})} r\,d\theta\,dr,\\
\frac{\partial \tilde{a}}{\partial t} &= \alpha a.
\end{aligned} \tag{20}$$

Here, $a(\underline{x}, t)$, $p(\underline{x}, t)$, $\tilde{a}(\underline{x}, t)$ are the densities of the cell types A, P, and $\tilde{A}$, respectively, at two-dimensional position $\underline{x}$ and time t, α is the rate at which differentiating cells a become differentiated cells $\tilde{a}$, f is as described in Fig. 2(a) and k is a positive constant.

We could again vary our contact function f to explore which contact scenario produces the results witnessed by Gurdon, and hence which is most likely to be the method adopted by *Xenopus* during myogenesis. More specifically, there is experimental data regarding the size of the initial precursor population that is necessary for differentiation via the community effect to take place (see Gurdon et al. 1993a), and the time it takes to occur. The model could use this data to obtain estimates of the distances over which these cells can sense their local cellular environment. Note that in this experiment the population of undifferentiated precursor cells is not constant. Therefore, our differentiation term in (20) is proportional to the varying population P, and this is an important difference from the corresponding term in (5). Note also that our integral term I_p calculates the proportion of undifferentiated precursor cells out of all cells present, including fully differentiated cells $\tilde{A}$. Thus, the true proportion of P cells within the sensing radius is considered: this is essential to create Gurdon's threshold effect.

We could also use the model to explore homoiogenetic induction, as discussed in Sect. 1 (see also Nieuwkoop 1997; Gurdon et al. 1993b). Here, we would simply have two cell populations: the precursors P and the differentiated cells A. The appropriate model would have a very similar form to that discussed for Gurdon's experiments above, but without the equation for $\tilde{a}$. The main difference would be in the integral term: I_p would be replaced with the term I_a, as homoiogenetic induction is brought about by the presence of differentiated cells, not by a precursor threshold. Using such a model would again allow us to uncover in more detail the relationships between various components of the process, as discussed above.

Other future work could involve analysing heterogeneous steady states to explore the structure and scale of patterns. This would enable us to investigate more fully the spatial aspects of zebrafish pigmentation stripes and in other examples, allowing us to look at the sharpness of the interface between stripes. Extending the model to three dimensions would allow better comparisons with experimental work, as would considering the corresponding model on a growing domain. Since fish are indeed three-dimensional and—in development—grow quite rapidly, we would expect such a model to more closely represent the *in vivo* scenario, and one could explore how stripe formation is affected by the stretching of the domain as the fish grows and changes shape. Again, we could adjust parameter values to explore their effect on the outcomes: for example altering the cell sensing radius may affect the width of stripes on a growing, curved domain. Furthermore, for better direct comparisons with experimental data, one could attempt a continuous model that is more closely derived from a discrete framework, allowing for the direct application of experimentally derived parameter values. Considering the effects of other cellular processes such as cellular attraction is also a possibility for a more complete model of cellular differentiation. Since our model's very generality means that it can be adjusted to fit numerous biological scenarios as demonstrated above, we hope it will be used to provide further insight into cell differentiation dynamics.

Acknowledgements J.M. Bloomfield was supported by a Doctoral Training Account Studentship from EPSRC. K.J. Painter and J.A. Sherratt were supported in part by Integrative Cancer Biology Program Grant CA113004 from the US National Institute of Health, and in part by BBSRC and EPSRC funding to the Centre for Systems Biology at Edinburgh. J.A. Sherratt was supported in part by a Leverhulme Trust Research Fellowship.

Appendix

In Fig. 11, we present results on the dynamics that arise when a circular "island" of one cell type is introduced into a "sea" of another type. The number of simulations required for this figure made two-dimensional simulations unfeasible. Therefore, we considered the case of the "island" being in the centre of a circular domain. The circular symmetry then makes the problem one-dimensional. However, the reduction to one dimension is somewhat involved, and we outline the details here.

We define x as a radial co-ordinate measured from the centre of the domain, and we denote by $\mathcal{C}(x)$ the circle, radius R, centred at x. We begin by considering the case $x > R$. We wish to calculate

$$I = \iint_{\mathcal{C}(x)} F(x),$$

where $F(x)$ is the integrand in question. So, in the calculation of Fig. 11, $F(x) = a(x)/(a(x) + b(x))$ for our population of A cells. Then

$$I = \int_{r=x-R}^{r=x+R} L(r)F(r)\,dr$$

where $L(r)$ is the length of the arc $\mathcal{L}(r)$ contained within $\mathcal{C}(x)$ of the circle centred at the origin, with radius r; we refer to this circle as $\mathcal{A}$. Then the end points of $\mathcal{L}(r)$ are $(r\cos\theta, r\sin\theta)$ and $(r\cos\theta, -r\sin\theta)$, the intersection points with $\mathcal{C}$ (Fig. 13(a)). Thus, $L = 2\theta r$, where

$$\theta = \arccos\bigl(1 - \bigl(R^2 - (r-x)^2\bigr)/2xr\bigr)$$

$$\Rightarrow \quad I = 2\int_{r=x-R}^{r=x+R} \arccos\left(1 - \frac{R^2 - (r-x)^2}{2xr}\right) r F(r)\,dr.$$

Note that the size of 'island' in the initial conditions does not affect this calculation at all: all arc lengths are centred at the origin and calculated appropriately according to the size of R, with the largest $\mathcal{A}$ marking the boundary of our original domain; the cell types present within the integral are considered purely in F, and their presence or otherwise should not be confused with the integration described. In particular the circle $\mathcal{A}$, which is used to calculate arc lengths, should not be confused with 'island' size.

The arguments above only apply if $x > R$. If $x \leq R$, the origin $x = 0$ lies inside $\mathcal{C}$, and for sufficiently small r the entire circle $\mathcal{A}$ lies inside $\mathcal{C}$. At the transition point

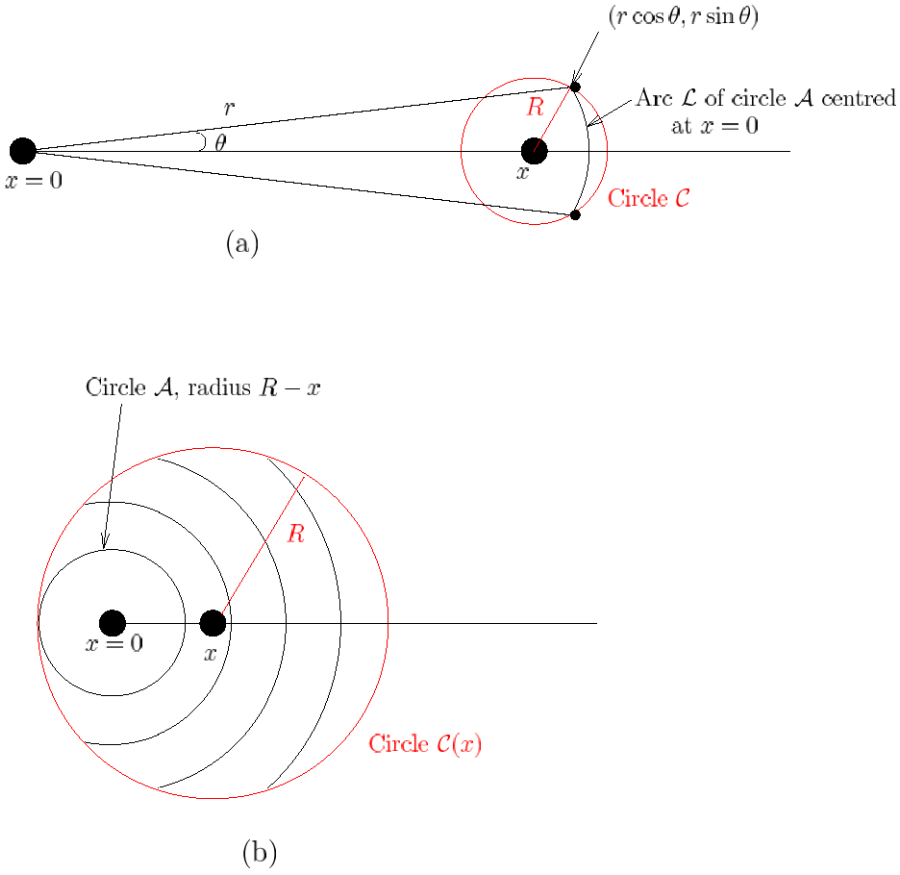

Fig. 13 Figure (**a**): Geometry of integral computation when $x - R$ is large. See text for details. Figure (**b**): Geometry of integral computation near to the origin 0, shown large to allow more detail. If $x - R \leq 0$, the arcs $\mathcal{L}(r)$ of $\mathcal{A}$, three of which are shown (and each of which are distance r away from the origin), eventually form a circle. At the transition point between arcs and circumferences, $\mathcal{C}$ and $\mathcal{A}$ touch, and the radius is given by $R - x$. See text for further details

between arcs and circumferences, $\mathcal{C}$ and $\mathcal{A}$ touch, and the radius is given by $R - x$ (Fig. 13(b)). Then

$$I = 2\int_{r=0}^{r=R-x} \pi r F(r)\, dr + 2\int_{r=R-x}^{r=x+R} \arccos\left(1 - \frac{R^2 - (r-x)^2}{2xr}\right) r F(r)\, dr.$$

A simple test of the formulae above is given by considering $F = 1$, in which case $I = \pi R^2$. For $R = 1$, we find that in order for the one-dimensional formulae to give the answer π correct to 3 significant figures, we must set the spatial discretisation to $\delta x = 0.01$. The computational speed-up arising from the one-dimensional formulae is considerable. A typical simulation required for Fig. 11 takes several hours in two dimensions but only 1 to 2 minutes in one dimension at the same accuracy level (for a 3.2 GHz processor with 4096 megabytes of memory).

References

Armstrong, N. J., Painter, K. J., & Sherratt, J. A. (2006). A continuum approach to modelling cell-cell adhesion. *J. Theor. Biol.*, *243*, 98–113.

Armstrong, N. J., Painter, K. J., & Sherratt, J. A. (2009). Adding adhesion to a chemical signalling model for somite formation. *Bull. Math. Biol.*, *71*(1), 1–24.

Atkinson, S., & Williams, P. (2009). Quorum sensing and social networking in the microbial world. *J. R. Soc. Interf.*, *6*, 959–978.

Aubin-Houzelstein, G., Bernex, F., Elbaz, C., & Panthier, J. J. (1998). Survival of patchwork melanoblasts is dependent upon their number in the hair follicle at the end of embryogenesis. *Dev. Biol.*, *198*, 266–276.

Bloomfield, J. M., Sherratt, J. A., Painter, K. J., & Landini, G. (2010). Cellular automata and integro-differential equation models for cell renewal in mosaic tissues. *J. R. Soc. Interf.* doi:10.1098/rsif.2010.0146.

Buckingham, M. (2003). How the community effect orchestrates muscle differentiation. *Bioessays*, *25*, 13–16.

Caicedo-Carvajal, C. E., & Shinbrot, T. (2008). In silico zebrafish pattern formation. *Dev. Biol.*, *315*(2), 397–403.

Cossu, G., Kelly, R., Di Donna, S., Vivarelli, E., & Buckingham, M. (1995). Myoblast differentiation during mammalian somitogenesis is dependent upon a community effect. *Proc. Natl. Acad. Sci. USA*, *92*(6), 2254–2258.

Galli, R., Borello, U., Gritti, A., Minasi, M. G., Bjornson, C., Coletta, M., Mora, M., De Angelis, M. G., Fiocco, R., Cossu, G., & Vescovi, A. L. (2000). Skeletal myogenic potential of human and mouse neural stem cells. *Nature Neurosci.*, *3*, 986–991.

Gerisch, A. (2010). On the approximation and efficient evaluation of integral terms in PDE models of cell adhesion. *IMA J. Numer. Anal.*, *30*, 173–194.

Gerisch, A., & Chaplain, M. (2008). Mathematical modelling of cancer cell invasion of tissue, Local and non-local models and the effect of adhesion. *J. Theor. Biol.*, *250*(4), 684–704.

Green, J. E. F., Waters, S. L., Whiteley, J. P., Edelstein-Keshet, L., Shakesheff, K. M., & Byrne, H. M. (2010). Non-local models for the formation of hepatocyte-stellate cell aggregates. *J. Theor. Biol.* DOI:10.1016/j.jtbi.2010.08.013.

Gurdon, J. B. (1988). A community effect in animal development. *Nature*, *336*, 772–774.

Gurdon, J. B., Lemaire, P., & Kato, K. (1993a). Community effects and related phenomena in development. *Cell*, *75*, 831–834.

Gurdon, J. B., Tiller, E., Roberts, J., & Kato, K. (1993b). A community effect in muscle development. *Curr. Biol.*, *3*, 1–11.

Hillen, T., & Painter, K. J. (2009). A user's guide to PDE models for chemotaxis. *J. Math. Biol.*, *58*, 183–217.

Hultman, K. A., & Johnson, S. L. (2010). Differential contribution of direct-developing and stem cell-derived melanocytes to the zebrafish larval pigment pattern. *Dev. Biol.*, *337*(2), 425–431.

Kaneko, T., Kojima, K., & Yasuda, K. (2007). Dependence of the community effect of cultured cardiomyocytes on the cell network pattern. *Biochem. Biophys. Res. Commun.*, *356*(2), 494–498.

Kato, K., & Gurdon, J. B. (1993). Single-cell transplantation determines the time when Xenopus muscle precursor cells acquire a capacity for autonomous differentiation. *Proc. Natl. Acad. Sci. USA*, *90*, 1310–1314.

Kim, D., Chi, S., Lee, K. H., Rhee, S., Kwon, Y. K., Chung, C. H., Kwon, H., & Kang, M. S. (1999). Neuregulin stimulates myogenic differentiation in an autocrine manner. *J. Biol. Chem.*, *274*, 15395–15400.

Kojima, K., Kaneko, T., & Yasuda, K. (2006). Role of the community effect of cardiomyocyte in the entrainment and reestablishment of stable beating rhythms. *Biochem. Biophys. Res. Commun.*, *351*(1), 209–215.

Kondo, S., Iwashita, M., & Yamaguchi, M. (2009). How animals get their skin patterns, fish pigment pattern as a live Turing wave. *Int. J. Dev. Biol.*, *53*, 851–856.

Maderspacher, F., & Nusslein-Volhard, C. (2003). Formation of the adult pigment pattern in zebrafish requires leopard and obelix dependent cell interactions. *Development*, *130*(15), 3447–3457.

Monk, N. (1997). The community effect and ectoderm–mesoderm interaction in Xenopus muscle differentiation. *Bull. Math. Biol.*, *59*(3), 409–425.

Moreira, J., & Deutsch, A. (2005). Pigment pattern formation in zebrafish during late larval stages, A model based on local interactions. *Dev. Dyn.*, *232*(1), 33–42.

Nagai, T., Otani, S., Saito, T., Maegawa, S., Inoue, K., Arai, K., & Yamaha, E. (2005). Germ-line chimera produced by blastoderm transplantation in zebrafish. *Nippon Suisan Gakkaishi*, *71*(1), 1–9.

Nieuwkoop, P. D. (1997). Short historical survey of pattern formation in the endo-mesoderm and the neural anlage in the vertebrates, the role of vertical and planar inductive actions. *Cell. Mol. Life Sci.*, *53*, 305–318.

Painter, K. J., Armstrong, N. J., & Sherratt, J. A. (2010). The impact of adhesion on cellular invasion processes in cancer and development. *J. Theor. Biol.*, *264*, 1057–1067.

Paratore, C., Hagedorn, L., Floris, J., Hari, L., Kleber, M., Suter, U., & Sommer, L. (2002). Cell-intrinsic and cell-extrinsic cues regulating lineage decisions in multipotent neural crest-derived progenitor cells. *Int. J. Dev. Biol.*, *46*(1), 193–200. Sp. Iss. SI.

Parichy, D. M. (2007). Homology and the evolution of novelty during Danio adult pigment pattern development. *J. Exp. Zool. B*, *308*(5), 578–590.

Parichy, D. M., Ransom, D. G., Paw, B., Zon, L. I., & Johnson, S. L. (2000). An orthologue of the kit-related gene fms is required for development of neural crest-derived xanthophores and a subpopulation of adult melanocytes in the zebrafish, Danio rerio. *Development*, *127*, 3031–3044.

Rawls, J., & Johnson, S. (2000). Zebrafish kit mutation reveals primary and secondary regulation of melanocyte development during fin stripe regeneration. *Development*, *127*(17), 3715–3724.

Salazar-Ciudad, I., Jernvall, J., & Newman, S. A. (2003). Mechanisms of pattern formation in development and evolution. *Development*, *130*, 2027–2037.

Sekimura, T., Zhu, M., Cook, J., Maini, P. K., & Murray, J. D. (1999). Pattern formation of scale cells in Lepidoptera by differential origin-dependent cell adhesion. *Bull. Math. Biol.*, *61*, 807–828.

Sherratt, J. A., Gourley, S. A., Armstrong, N. J., & Painter, K. J. (2009). Boundedness of solutions of a non-local reaction-diffusion model for adhesion in cell aggregation and cancer invasion. *Eur. J. Appl. Math.*, *20*(1), 123–144.

Standley, H. J., Zorn, A. M., & Gurdon, J. B. (2001). eFGF and its mode of action in the community effect during xenopus myogenesis. *Development*, *128*(8), 1347–1357.

Watt, F. M., Lo Celso, C., & Silva-Vargas, V. (2006). Epidermal stem cells, an update. *Curr. Opin. Genet. Dev.*, *16*, 518–524.

Weiner, R., Schmitt, B. A., & Podhaisky, H. (1997). ROWMAP—A ROW-code with Krylov techniques for large stiff ODEs. *Appl. Numer. Math.*, *25*(2), 303–319.

Weston, M. J. D., Kato, K., & Gurdon, J. B. (1994). A community effect is required for amphibian notochord differentiation. *Dev. Genes Evol.*, *203*(5), 250–253.

Yamaguchi, M., Yoshimoto, E., & Kondo, S. (2007). Pattern regulation in the stripe of zebrafish suggests an underlying dynamic and autonomous mechanism. *Proc. Natl. Acad. Sci. USA*, *104*(12), 4790–4793.

Yang, H., Jensen, P., & Goldowitz, D. (2002). The community effect and purkinje cell migration in the cerebellar cortex, analysis of scrambler chimeric mice. *J. Neurosci.*, *22*(2), 464–470.

Zhong, W. (2008). Timing cell-fate determination during asymmetric cell divisions. *Curr. Opin. Neurobiol.*, *18*, 472–478.